Soil Dynamics and Earthquake Engineering 122 (2019) 94–106

Contents lists available at ScienceDirect

Soil Dynamics and Earthquake Engineering

journal homepage: www.elsevier.com/locate/soildyn

Prediction models and seismic hazard assessment: A case study from Taiwan

Yun Xu[a], J.P. Wang[b,*], Yih-Min Wu[c], Hao Kuo-Chen[d]

[a] Dept. Civil & Environmental Eng., Hong Kong University of Science and Technology, China
[b] Dept. Civil Engineering, National Central University, Taiwan
[c] Dept. Geosciences, National Taiwan University, Taiwan
[d] Dept. of Earth Sciences and Institute of Geophysics, National Central University, Taiwan

ARTICLE INFO

Keywords:
CAV
Prediction equation
Seismic hazard
Taiwan

ABSTRACT

Proposed in the late 1980s, cumulative absolute velocity (CAV) is a new intensity measure for earthquake ground motion characterizations, followed by studies and applications such as CAV ground motion prediction equations (GMPEs). In this study, two new CAV GMPEs were developed with 24,667 strong-motion records from Taiwan, and the first CAV seismic hazard assessment for Taipei (the most important city in Taiwan) was then conducted using the local CAV models. It shows that the annual rate for the study area to encounter a ground motion with CAV > 0.97 g-sec is 0.002 per year, corresponding to a 10% occurrence probability in 50 years. By contrast, the deterministic scenario-based analysis shows that the CAV seismic hazard is about 0.60 g-sec for the study area. Future studies are worth conducting to develop more sophisticated, local CAV GPMEs and to explore more applications of such CAV prediction models, such as the developments of PGA-CAV joint probability distributions for conducting PGA-CAV joint seismic hazard assessments.

1. Introduction

Earthquakes generate random ground motions governed by a variety of uncertainties (e.g., source mechanisms, wave propagation path, site condition, topography, etc.). In order to characterize the intensity of an earthquake, many intensity measures (IMs) were proposed [1], such as peak ground acceleration (PGA) and response spectral acceleration (SA) that are commonly used for earthquake-resistant design. For estimating the levels of PGA/SA during earthquakes, ground motion prediction equations (GMPEs) were developed and calibrated with instrumental data [e.g., Refs. [2–7]]. For example, several PGA GMPEs were developed based on the NGA (Next Generation of Ground-Motion Attenuation Models) database [2–5], with others developed based on local data from Greece and Taiwan [6,7].

Proposed in the late 1980s, cumulative absolute velocity (CAV) is a new intensity measure for earthquake ground motion characterizations. Different from PGA/SA based on a motion's peak amplitude only, CAV is a result of the whole acceleration time history that was first proposed by the Electric Power Research Institute (EPRI) to improve post-earthquake inspection on nuclear power plants [8]. Specifically, the motivation was originated from realizing three nuclear power plants, which were nonoperational at that time, would had been requested a shutdown by U.S. Nuclear Regulatory Commission (USNRC) for post-earthquake inspection, even though the plants were clearly not affected. For better addressing the issue, EPRI led a research project studying the correlation between structural damages and several IMs; then based on 250 earthquake records, CAV was found as the most suitable indicator/predictor to structural damage among the IMs examined [8].

According to EPRI, the mathematical formulation of CAV was defined as follows [8]:

$$CAV = \int_0^{t_{\max}} |a(t)|dt \tag{1}$$

where $|a(t)|$ denotes the absolute value of acceleration at time t, and $t_{\max}$ is the duration of the ground motion. Fig. 1a illustrates the calculation of CAV for a hypothetical motion. As the shaded area shown, CAV is an intensity measure based on the whole acceleration time history, considering the cumulative effect of an earthquake ground motion.

Later on, different versions of CAV were proposed for excluding CAV contributions from small amplitudes that are unlikely to cause structural damage [e.g., Refs. [9–11]]. For example, one derivative, referred to as $\mathbf{CAV_{CUTOFF}}$ herein (Fig. 1b), is expressed as follows [9,10]:

$$CAV_{\mathrm{CUTOFF}} = \sum_{i=1}^{N} H(pga_i - pga_{\mathrm{cutoff}}) \int_{t=t_i}^{t_{i+1}} |a(t)|dt \tag{2}$$

* Corresponding author.
E-mail address: jpwang@ncu.edu.tw (J.P. Wang).

https://doi.org/10.1016/j.soildyn.2019.03.038
Received 10 December 2018; Accepted 26 March 2019

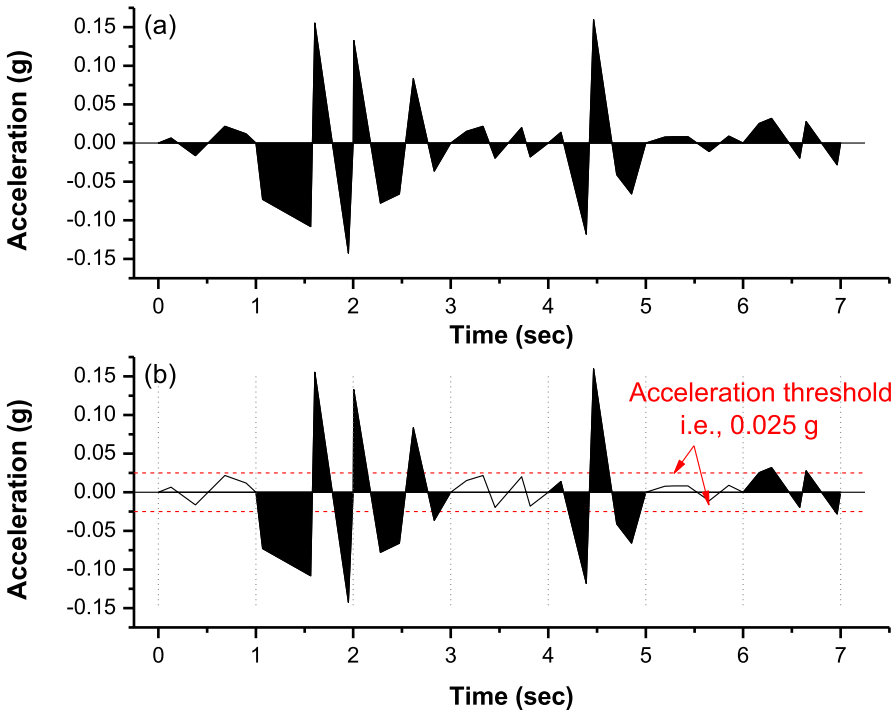

Fig. 1. CAV (cumulative absolute velocity) of a hypothetical acceleration time history that is equal to the summation of the shaded area: a) CAV and b) $CAV_{CUT-OFF} = 0.025$ g.

where N is the total duration of a ground motion in seconds, pga_i is the maximum acceleration (absolute value) in the i-th second of the motion, pga_{cutoff} is the acceleration cutoff value, and H() is the Heaviside function:

$$H(x) = \begin{cases} 1, & x \geq 0 \\ 0, & x > 0 \end{cases} \tag{3}$$

Note that the cutoff thresholds of 0.025 g and 0.02 g were proposed in different studies [9,10].

Correlation between CAV and structural damage has been examined since then. EPRI found that CAV was a good indicator to Modified Mercalli Intensity (MMI) VII, a level that damages on buildings of good design starts to occur [8]. Similarly, Cabañas et al. [10] found a strong correlation between $CAV_{CUTOFF = 0.02\,g}$ and the local macroseismic intensity in Italy, while Koliopoulos et al. [12] noted that CAV and Housner Intensity [13] were well correlated based on data from Greece. Then Kostov [14] concluded CAV should be a better indicator than PGA to structural damage, based on more instrumental data and field observations. Moreover, Campbell and Bozorgnia further investigated the correlation between the standardized CAV and Japan Meteorological Agency (JMA) and MMI macroseismic intensity scales, characterizing the thresholds of standardized CAV associated with the onsets of damage to structures of good design and construction, one of the important findings and contributions from the study [15].

As PGA/SA GMPEs, several CAV models were developed for CAV predictions. The models include those proposed by Danciu and Tselentis [6] based on data from Greece, and those by Campbell and Bozorgnia considering styles of faulting and rupture depth into their model development [16,17]. In addition, for increasing such a model's applicability Du and Wang [18] developed a CAV GMPE in a simpler functional form. Notably, it has been consistently pointed out that the standard deviation of CAV GMPEs is smaller than that of a series of GMPEs for PGA, SA, AI (Arias Intensity), etc., even developed with the same functional form and the same pool of earthquake data [e.g., 6, 19].

Although several CAV GMPEs as mentioned above have been proposed and local PGA GMPEs have been developed for the area of Taiwan [7], not a local CAV model was developed for the area. As a result, the key scope of the study is to develop the first CAV GMPEs for Taiwan. Specifically, the data from the Taiwan Strong Motion Instrumentation Program (TSMIP) were collected and used. We also conducted the first CAV seismic hazard study for Taipei (the most important city in Taiwan) using the CAV models developed, another highlight and contribution of the study.

2. Taiwan Strong Motion Instrumentation Program, TSMIP

2.1. Overview

Located on the boundaries of three tectonic plates, the region around Taiwan is known for high seismicity. Statistics show that around 2,000 earthquakes above M_L 3.0 (local magnitude) can be occurring in the region every year, and a catastrophic event like the M_L 7.3 Chi-Chi earthquake in 1999 could recur in decades [20]. As a result, a variety of earthquake studies, such as earthquake early warning [e.g., Ref. [21]], seismic hazard analysis [e.g., Refs. [22,23]], and earthquake probability evaluation [e.g., Refs. [24–26]], were conducted for the region around Taiwan.

In order to gather more seismic data, the Taiwan Strong Motion Instrumentation Program, TSMIP, was launched in the 1990s, building many earthquake stations in order to collect ground motion data. As of now, TSMIP has 688 free-field earthquake stations in operation [27], with each capable of recording ground motions in three directions with a sampling rate of 200 or 250 per second [28]. It is also worth noting that around 100 stations among them are equipped with automatic data transmitting systems that can send data to the Central Weather Bureau Taiwan immediately for some real-time analyses, like earthquake early warning [29].

Based on the NEHRP (National Earthquake Hazards Reduction Program) provisions, 439 of the stations were investigated and categorized into one of the following site conditions: 1) Type A: hard-rock site with Vs30 > 1500 m/s, where Vs30 is the average shear-wave

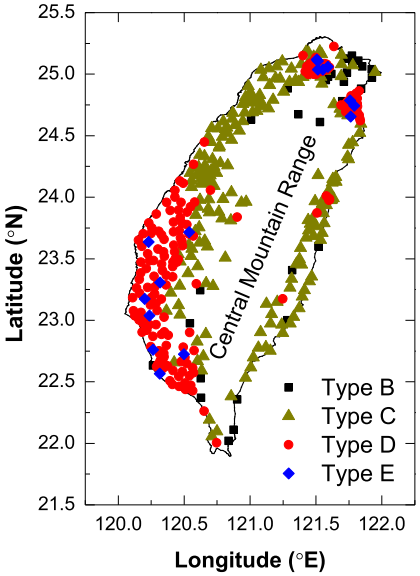

Fig. 2. Spatial distribution of the 439 classified stations of the Taiwan Strong Motion Instrumentation Program (TSMIP) ([28]).

velocity in the top 30 m below the ground surface; 2) Type B: firm-to hard-rock site with Vs30 from 760 to 1500 m/s; 3) Type C: dense-soil and soft-rock site with Vs30 from 360 to 760 m/s; 4) Type D: stiff-soil site with Vs30 ranging from 180 to 360 m/s; and 5) Type E: soft-soil site with Vs30 < 180 m/s. Fig. 2 shows the distribution of the 439 stations with known site conditions. For more details on the site investigations and characterizations, refer to Kuo et al. [30].

The TSMIP database becomes invaluable to earthquake studies, especially those focusing on Taiwan. For example, Sokolov et al. [31] used the local database to investigate the basin effect in Taipei on site amplification during earthquakes. For earthquake early warning, the "high-density" instrumental network is the key to the success of a local system that can issue warnings as soon as 20 s after the occurrence/initiation of earthquake [32]. Moreover, the database also provides opportunities for cross-checking the earthquake models that have been developed. For instance, Xu et al. [33] reported that the reliability of an on-site earthquake early warning implemented in Taiwan was around 85%, calculated by counting the numbers of missed alarm and false alarm based on 40,000 plus tests using TSMIP ground motions substituted into the decision-making criteria. Other TSMIP-based studies include local ground motion model developments [7] and earthquake statistical study for Taiwan [34].

2.2. Data collection and processing

Since the 1990s, TSMIP has recorded a lot of (raw) data in the format of acceleration time histories. As a result, our first task is to gather the data of our interest under following conditions: 1) motions from stations with known site conditions were collected for incorporating site effect into model developments; 2) motions associated with magnitude above M_w 4.8 (moment magnitude) and within 200 km from epicenters were collected, screening out less severe motions that are incapable of causing structure damage. Therefore, a total of 24,667 strong-motion data were collected from the local database, and it is the largest sample size by far for a GMPE study, to the best of our knowledge.

More details regarding the data set are as follows: 1) the 24,677 records are associated with 310 major earthquakes (moment magnitude

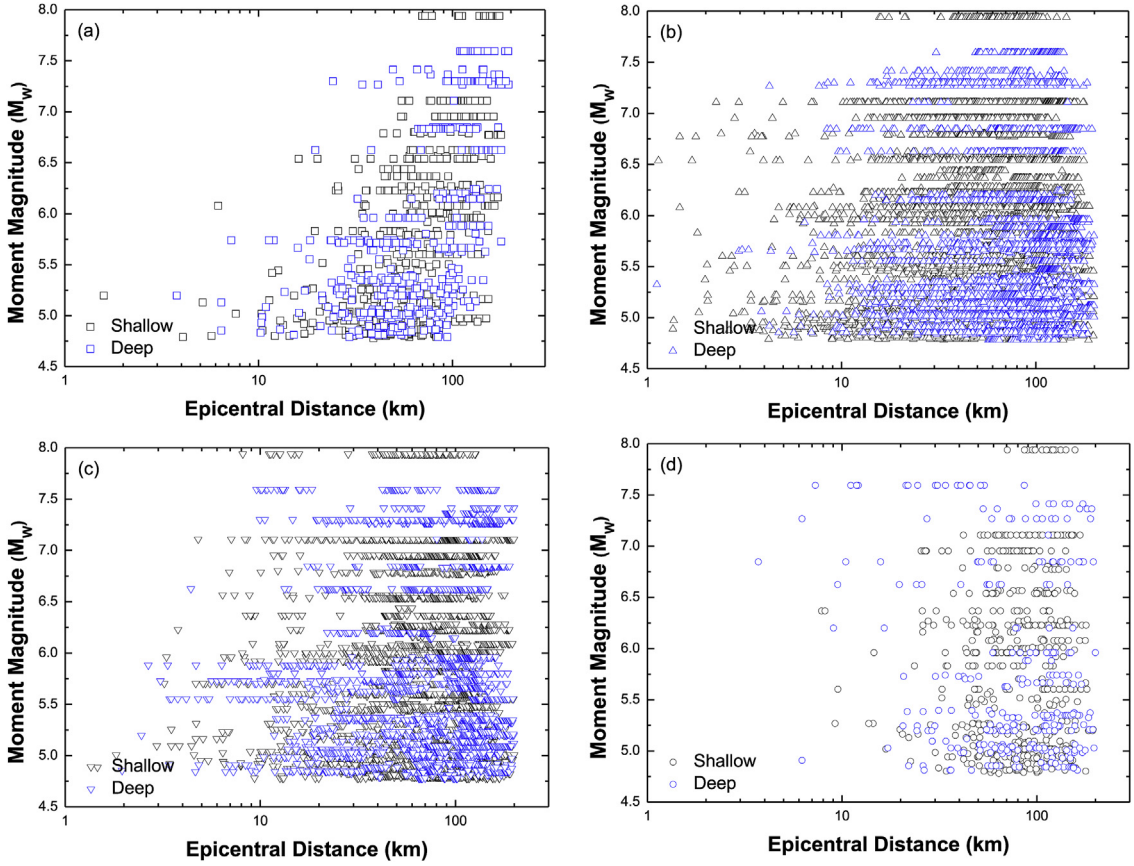

Fig. 3. Moment magnitude and epicentral distance of the 24,677 local strong-motion data used in this study: a) Type-B site condition, b) Type-C site condition, c) Type-D site condition, and d) Type-E site condition; note that the shallow-source and deep-source data are separated by a focal depth of 30 km.

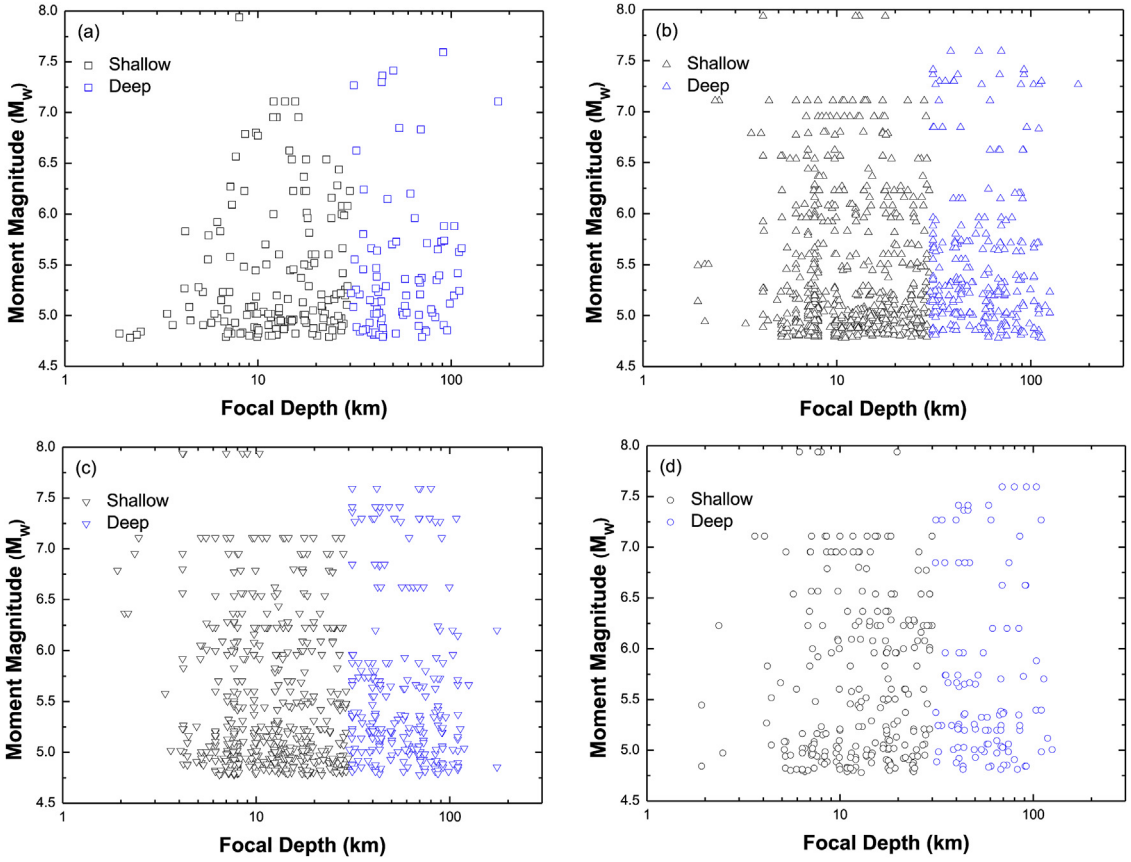

Fig. 4. Moment magnitude and focal depth of the strong-motion data used in this study: a) Type-B site condition, b) Type-C site condition, c) Type-D site condition, and d) Type-E site condition.

from M_w 4.8 to 7.9) since 1999; 2) focal depth ranges from 1 to 176 km; 3) earthquakes with focal depth less than 30 km are considered as shallow sources, otherwise as deep sources; 4) given TSMIP uses local magnitude, the moment magnitudes calculated and used were based on an empirical relationship [35]; and 5) given TSMIP not containing rupture data, the source-to-site distance calculated and used is epicentral distance but not rupture distance. Figs. 3 and 4 show the distributions of the data with respect to magnitude, epicentral distance, focal depth, and site condition.

After collecting the strong-motion data, the next is to calculate CAV of each motion. Following other studies [e.g., Refs. [15–19]], the geometric mean of two horizontal motions (i.e., East-West and North-South) was used in this study:

$$CAV = \sqrt{CAV_1 \times CAV_2} \tag{4}$$

where CAV_1 and CAV_2 denote the CAV in the North-South and East-West directions, respectively. Note that an in-house (MATLAB) program was developed for the massive data processing.

3. Local CAV GMPE for Taiwan

3.1. Model development

The methodology proposed by Abrahamson and Youngs [36] was used for developing the local CAV GMPEs for Taiwan:

$$\ln CAV_{ij} = \overline{\ln CAV_{ij}} + \eta_i + \varepsilon_{ij} \tag{5}$$

where $\ln CAV_{ij}$ and $\overline{\ln CAV_{ij}}$ denote observed and predicted lnCAV for the j-th record of the i-th event, respectively. Note that it separates the model errors (or uncertainties) into two parts: the inter-event variation for the i-th event, denoted as η_i, and the intra-event variation for the j-th record, denoted as ε_{ij}, and in theory they are statistically independent and both are normally distributed with mean = 0. As for standard deviation, τ (for η_i) and σ (for ε_{ij}) were calculated based on the level of scattering in the data set with the 24,677 records. Consequently, the total residuals of the model can be determined as:

$$\sigma_T = \sqrt{\tau^2 + \sigma^2} \tag{6}$$

After examining data distribution and considering data similarity [18], the following form was adopted:

$$\overline{\ln CAV_{ij}} = c_1 + c_2(8.5 - M_W)^2 + (c_3 + c_4 M_w)\ln\sqrt{D^2 + H^2} + c_5 \ln(Vs_{30}) + c_6 S_B + c_7 S_C + c_8 S_D + c_9 S_E \tag{7}$$

where M_W is moment magnitude, D is epicentral distance in km, H is focal depth in km, Vs_{30} is the average shear-wave velocity of soil/rock 30 m below the ground surface, c_1 to c_9 are model parameters calibrated with regression analytics, and S_B, S_C, S_D, and S_E are Boolean data (0 or 1) representing site conditions (e.g., when the data are associated with Type-B site condition, S_B is equal to 1 while the rest (i.e., S_C, S_D and S_E) are all equal to 0).

Table 1 summarizes the model parameters (i.e., c_1 to c_9), standard deviations, and coefficient of determination (R^2). It is worth noting that the R^2 values are 0.74 and 0.67 for the deep-source and shallow-source models. In other words, around 70% of the data variability can be explained by the regression model.

3.2. Model checking: inter-event and intra-event residuals

It is imperative to perform model checking on a regression model [37], usually assessed by the two criteria: 1) the distribution of residuals (i.e., observation subtracting prediction) should follow the normal distribution with mean = 0; and 2) residuals must be randomly

Table 1
Summary of the two CAV GMPEs for Taiwan developed with the TSMIP database.

Earthquake Source	Model parameters									τ[a]	σ[b]	R[b]	*Sample size*
	c_1	c_2	c_3	c_4	c_5	c_6	c_7	C_8	c_9				
Shallow	1.153	−0.117	−1.565	0.127	−0.114	0.465	0.978	1.245	1.465	0.335	0.475	0.67	17,171
Deep	0.974	0.064	−2.873	0.309	−0.208	1.087	1.485	1.542	1.467	0.187	0.485	0.74	7,496

[a] τ is the standard deviation of the inter-event residual, and.
[b] σ is the standard deviation of the intra-event residual.

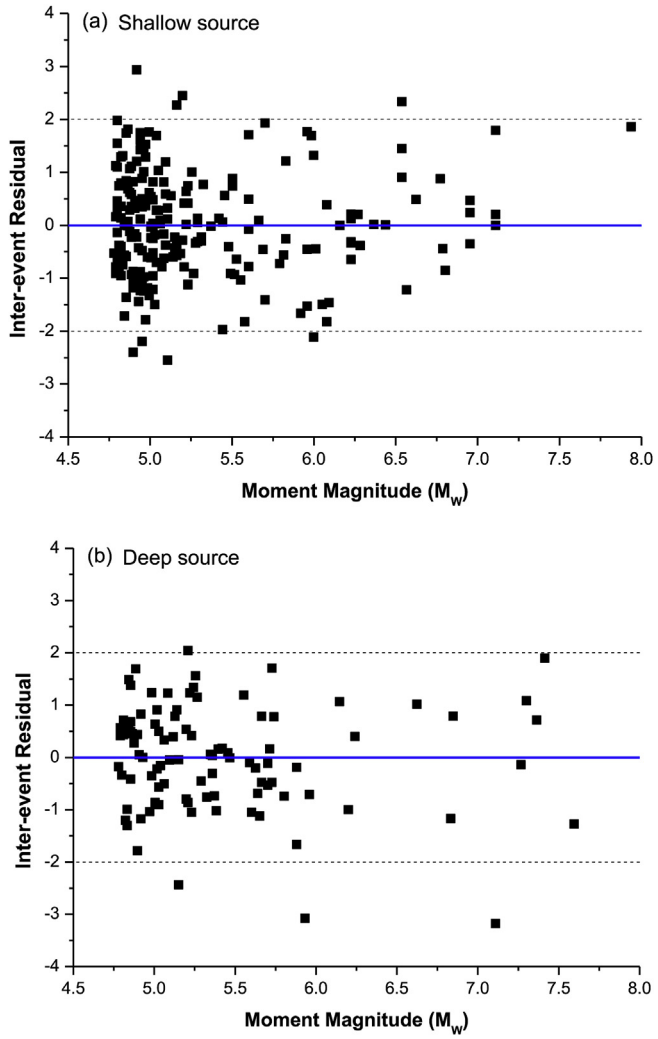

Fig. 5. Distribution of inter-event residuals against moment magnitude: a) shallow sources and b) deep sources.

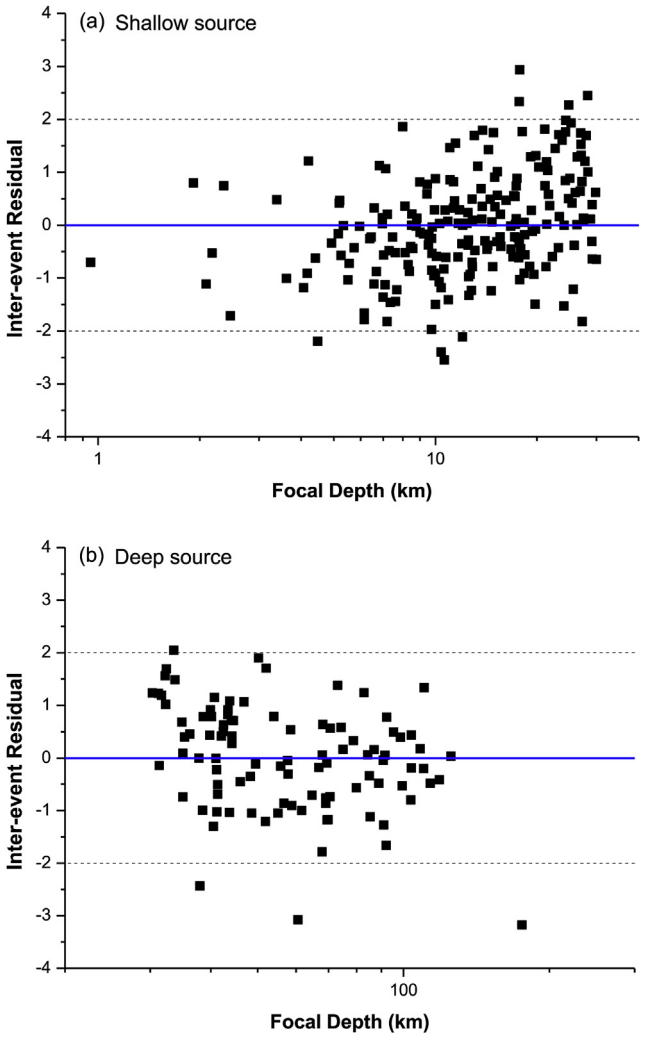

Fig. 6. Distribution of inter-event residuals against focal depth: a) shallow sources and b) deep sources.

distributed with little correlation with prediction variables. With the two criteria verified, the regression model is then considered robust.

Figs. 5 and 6 show the inter-event residuals with respect to magnitude and focal depth (two key independent variables of the regression model). It was found that the residuals are randomly distributed with little correlation with either magnitude or depth. Figs. 7–9 show the intra-event residuals against magnitude, epicentral distance and Vs30, with little correlation found either. Figs. 10 and 11 are the histograms of the residuals, demonstrating a bell-shaped distribution well simulating the normal distribution targeted. Therefore, the regression models should be robust based on the diagnostic plots, with residuals showing little correlation with independent variables and their distribution close to the normal distribution.

4. Model evaluation and comparison

Figs. 12–14 show the medians of CAV with respect to site condition, epicentral distance, and moment magnitude. It shows that the shallow-source model consistently predicts a greater CAV than the deep-source model does. In addition, as shown in Fig. 12, larger predictions appear as far as the Type-E site condition is concerned, followed by motions on Type-D, Type-C, and Type-B site conditions, revealing softer materials could amplify earthquake motions more extensively. For shallow-source models subject to M_w 6.5 as shown in Fig. 12a, CAV predictions attenuate nonlinearly with increasing distance; by contrast, the CAV predictions from the deep-source model shown in Fig. 12b are somehow saturated till 30 km from the epicenter, then attenuating more linearly with distance increasing from 30 km. On the condition of strong ground

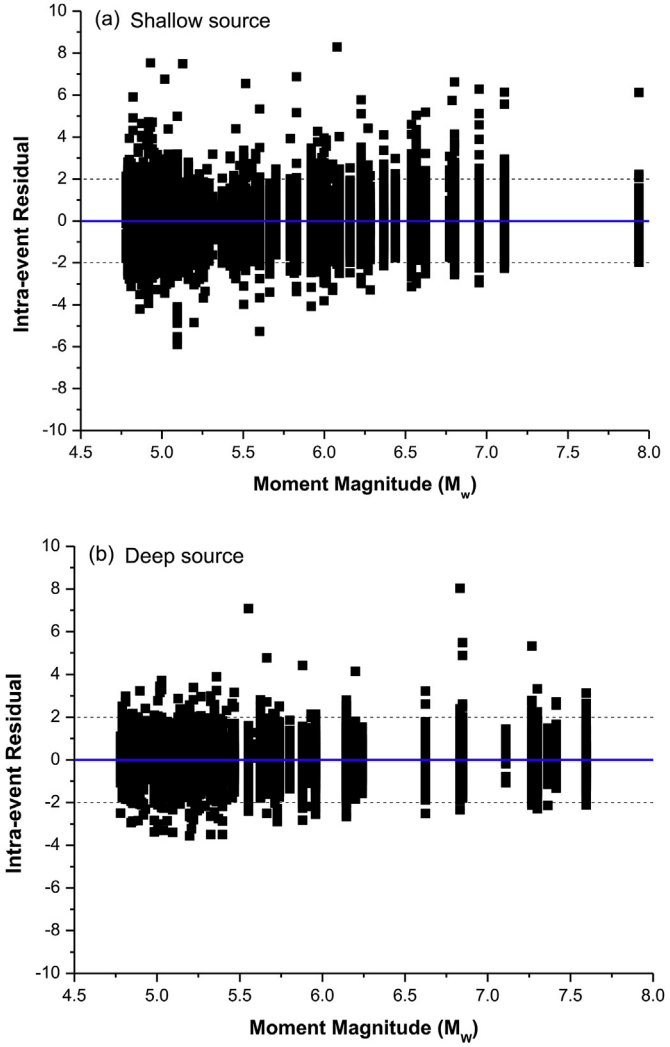

Fig. 7. Distribution of intra-event residuals against moment magnitude: a) shallow sources and b) deep sources.

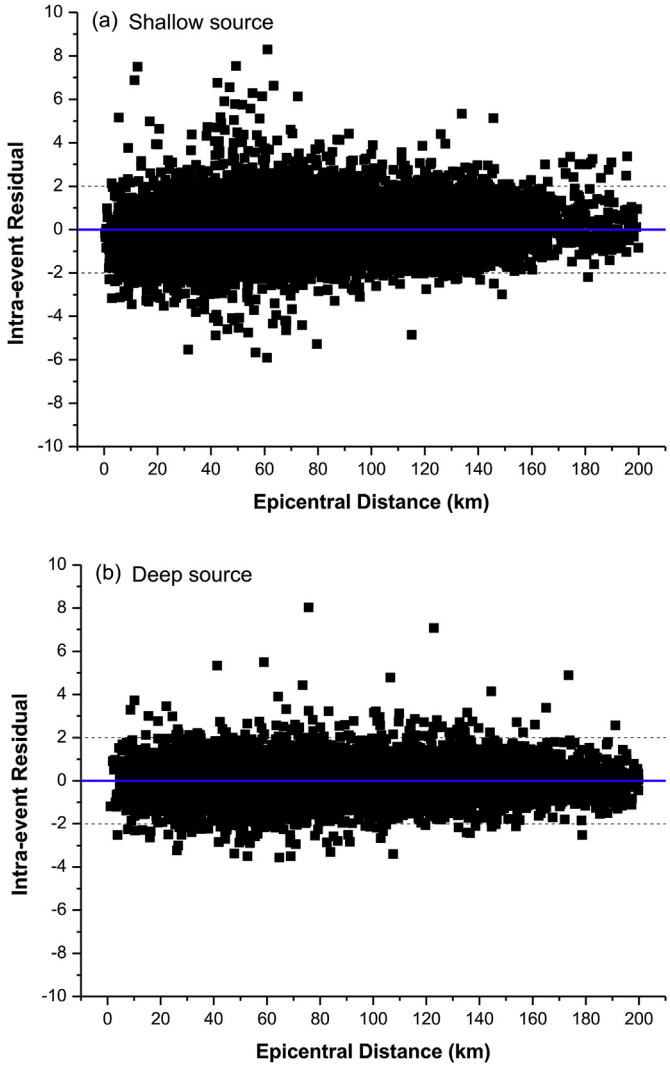

Fig. 8. Distribution of intra-event residuals against epicentral distance: a) shallow sources and b) deep sources.

shaking resulting from small source-to-site distance (e.g., < 30 km) and large magnitude (e.g., M_w > 6.5), the shallow-source model has the feature that the CAV increment because of site condition is nearly a constant, unlike the deep-source model that shows a large increment from Site B to Site C, while the site effect is almost saturated from a soft site (Site D) to a very soft site (Site E). Such features present in the CAV GMPEs are quite unique in comparison to models developed by Campbell and Bozorgnia [16,19] identifying CAV predictions could be amplified with site condition in a more nonlinear nature, but similar to the model developed by Du and Wang [18]. It is postulated that the difference in site amplification effect should be resulted from the adopted functional forms. More sophisticated functional forms could possibly capture more detailed site behavior, however, limiting the model's applicability. More studies are worth conducting to investigate the possible causes to such features present in the local model. On the other hand, owing to the uniqueness of a local model reflecting to the unique local geological background, it is better and more reasonable to adopt local models in follow-up applications to make the results more representative, which is also the key motivation of the study to develop the first CAV GMPE based on local data.

On the basis of using similar functional forms for the model developments, the model developed in this study, referred to as Model 2017, was first compared to the reference model referred to as Model 2012 [18]. The act is to provide some more justification to the new, local models for Taiwan that are able to predict CAV reasonably. However, the four underlying differences between the two must be noted because of the different formats in raw data: i) Model 2017 incorporates focal depth and Vs_{30} in model development; ii) Model 2017 incorporates the Type-B and Type-E site conditions; iii) Model 2017 uses epicentral distance; iv) Model 2017 does not incorporate styles of faulting.

Fig. 15 shows CAV predictions from the two models. In terms of the central value, overall Model 2012 predicts a greater CAV than Model 2017 does. Since earthquake induced ground motions are strongly influenced by focal depth and rupture direction (especially for near source and a major event), this difference should result from the facts that we used epicentral distance and did not account for faulting mechanisms in the model. However, this is the limitation that the TSMIP ground-motion database does not have rupture data and detailed focal mechanisms as mentioned previously. But overall speaking (from Fig. 15a–c), the CAV predictions from the two models are comparable, providing additional verification to the local model that predicts CAV reasonably.

Moreover, Model 2017 was further compared to the CAV GMPE developed by Campbell and Bozorgnia [19] based on NGA database. Note that the model development of the Campbell and Bozorgnia's model, referred to as Model 2010, is quite different and sophisticated, incorporating effect of fault mechanism, hanging wall, shallow site response, and basin effect. The comparison, as shown in Fig. 16,

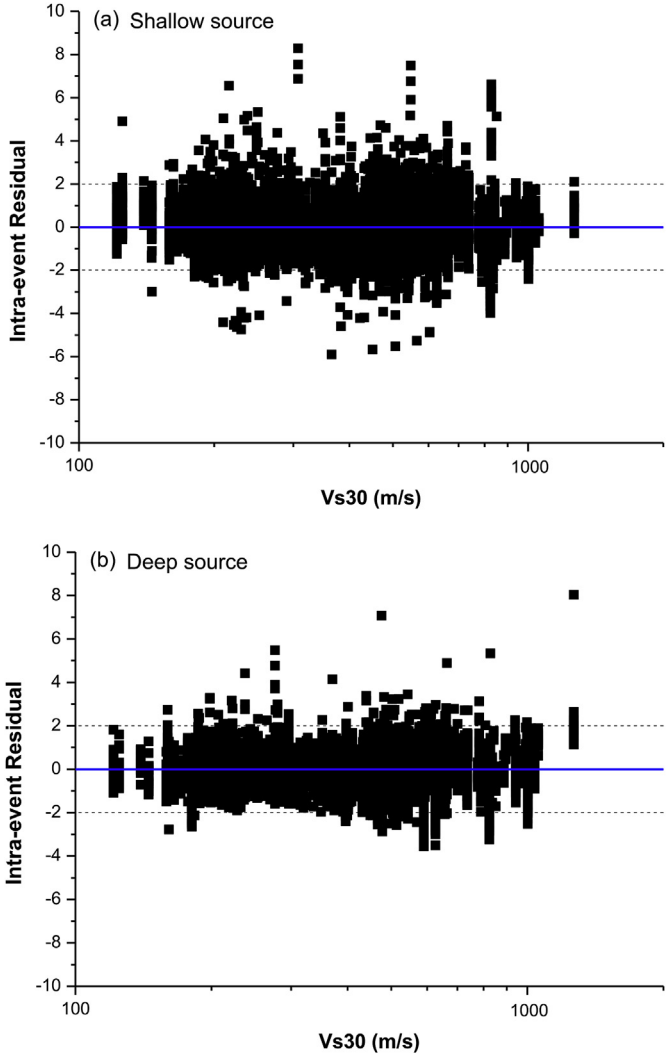

Fig. 9. Distribution of intra-event residuals against Vs30: a) shallow sources and b) deep sources.

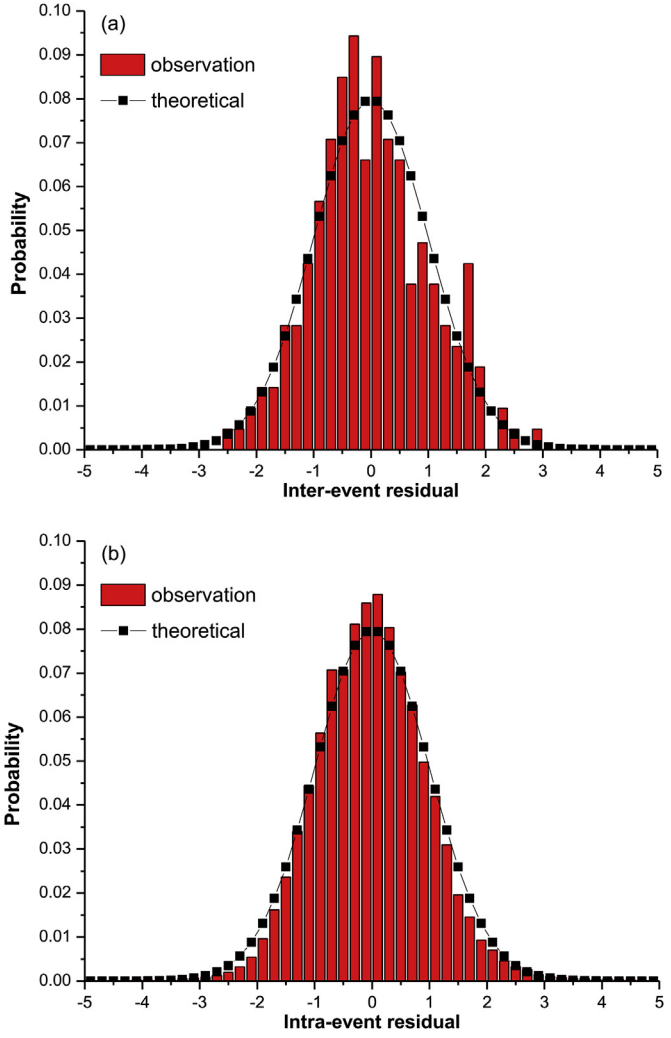

Fig. 10. Normal plot of inter-event and intra-event residuals from shallow sources: a) inter-event residual and b) intra-event residual.

indicates a larger estimate from Model 2010 than Model 2017. However, again, median estimates of CAV and the trend of CAV estimates are generally in agreement with each other. Considering very different database and different functional forms in the model development of Model 2010 and Model 2017, the difference in CAV predictions should be reasonable and acceptable.

In terms of aleatory uncertainty, Model 2017 has a larger standard deviation than Model 2012, or Model 2010, does. The possibilities to the result and the difference could be as follows: 1) epicentral distance used in Model 2017 could be less indicative to ground motion than rupture distance; 2) the ground motions used for developing Model 2017 are more diversified, including those associated with earthquakes in subduction zones of northeastern and southwestern Taiwan, and those from other geological regimes in central and western Taiwan; 3) an empirical relationship was used to convert local magnitude to moment magnitude, an additional source of uncertainty to Model 2017; and 4) the nature of ground motion attenuation in Taiwan is more random than other areas, probably owing to a more complicated geological background.

Based on the residual plots and the model comparison, the local CAV GMPE for Taiwan is considered mathematically robust, and capable of producing reasonable predictions as the reference. Future studies are worth investigating to compare it with more CAV GMPEs, although the comparison might be somewhat ambiguous if model basics are fundamentally different (e.g., epicentral distance *vs* rupture distance). To better address this, TSMIP is better to include rupture data and other focal mechanisms (especially for major events) in the future, so that new local models based on different formats of data can be further developed.

5. Discussion

5.1. Seismic hazard analysis

Seismic hazard analysis has become more important to (site-specific) earthquake-resistant design. On top of case studies [e.g., Refs. [38–44]], technical references, such as R.G. 1.208 of U.S. Nuclear Regulatory Commission (USNRC) [45], have prescribed it as the standard method for developing site-specific design parameters for nuclear power plants. Seismic hazard analysis can be mainly categorized into Probabilistic Seismic Hazard Analysis (PSHA) and Deterministic Seismic Hazard Analysis (DSHA) [46]. It is noted that "seismic hazard" is referred to as "*the likelihood of experiencing a specified* ***intensity*** *of any damaging phenomenon at a particular site*" [47,48], instead of economic loss or loss of life implicated from hazard.

- Overview of PSHA

The methodology and algorithm of PSHA can be summarized as

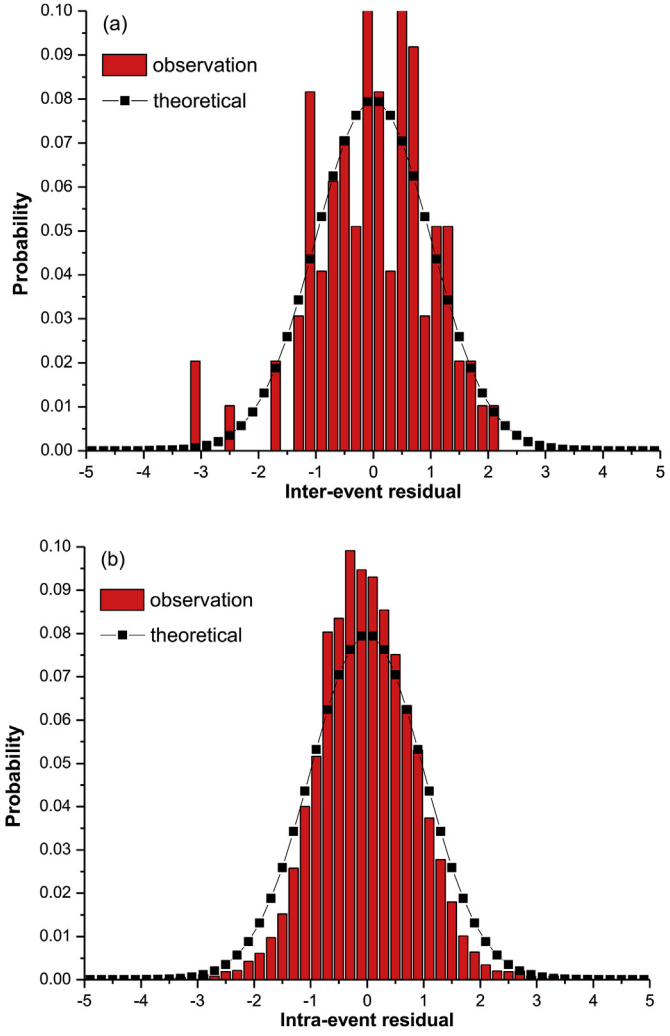

Fig. 11. Normal plot of inter-event and intra-event residuals from deep sources: a) inter-event residual and b) intra-event residual.

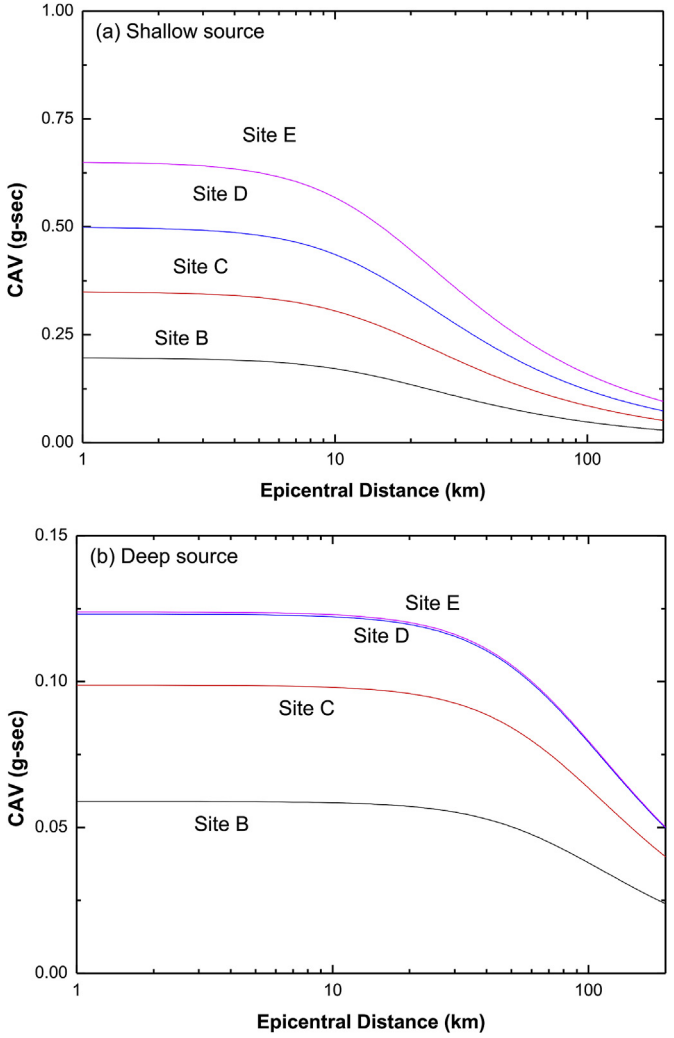

Fig. 12. Median predicted values of CAV with respect to site condition: a) shallow source and b) deep source; note that the median predicted CAV value is calculated with $M_W = 6.5$; Note that the focal depth for shallow and deep source is assumed to be 15 km and 75 km, respectively, and the Vs30 for site B, C, D, E is assumed to be 906, 512, 233, and 158 m/s, respectively.

follows: The performance function of the probabilistic analysis is usually a PGA or SA GMPE as PGA = f (M, D) + ε, where ε is the model's standard deviation (M is magnitude, and D is distance). Then the analysis is to estimate the exceedance probability of a certain level of ground shaking that a site would encounter, based on the uncertainties associated with the three variables (i.e., ε, M, and D). Note that PSHA uses total-probability algorithms as follows to calculate the exceedance Pr(PGA > y^*) [1], which can also be solved using Monte Carlo Simulation [49,50].

$$\Pr(PGA > y*) = \sum_{i=1}^{N_D}\sum_{j=1}^{N_M} \Pr(PGA > y* | D = d_i, M = m_j) \times \Pr(D = d_i) \times \Pr(M = m_j) \quad (8)$$

where N_M and N_D are the number of data bins in magnitude and distance probability functions as shown in Fig. 17a and b.

Fig. 17 is a systematic diagram showing the basics of PSHA computation: For a given magnitude and distance, the probability distribution of lnPGA (or PGA) can be estimated with a GMPE, so that the exceedance probability Pr(PGA > y^*) can be calculated as the highlighted area in Fig. 17c. With such calculation repeated using different magnitudes and distances with their probabilities also characterized (i.e., Fig. 17a and b), the total exceedance probability Pr(PGA > y^*) is then equal to the sum of exceedance probabilities associated with each scenario, as the equation expressed in Eq. (8).

The total exceedance probability calculated with Eq. (8) is seismic hazard contributed by one earthquake from one specific seismic zone. Therefore, when a site is surrounded by N_S sources with each's annual rate = v, the annual rate for the site to encounter a ground motion with PGA > y^*, denoted as $\lambda(PGA > y*)$, becomes as follows [1]:

$$\lambda(PGA > y*) = \sum_{k=1}^{N_S} v_k \times \Pr(PGA > y*) \quad (9)$$

To sum up, PSHA is a probabilistic analysis to estimate the annual rate of PGA exceedance considering the (aleatory) uncertainties of earthquake magnitude, location, and GMPE model error. The performance function is a PGA (or SA) GMPE, and the calculation is usually solved by using total-probability algorithms.

- Overview of DHSA

Deterministic Seismic Hazard Analysis, or scenario-based analysis, is relatively straightforward compared to PSHA. Different than PSHA considering magnitude and distance uncertainties, DSHA estimates seismic hazard subject to a worst-case scenario in term of (maximum) magnitude and (minimum) distance. Therefore, for a given PGA GMPE as PGA = f (M, D) ± σ_ε, the deterministic estimates from DSHA are

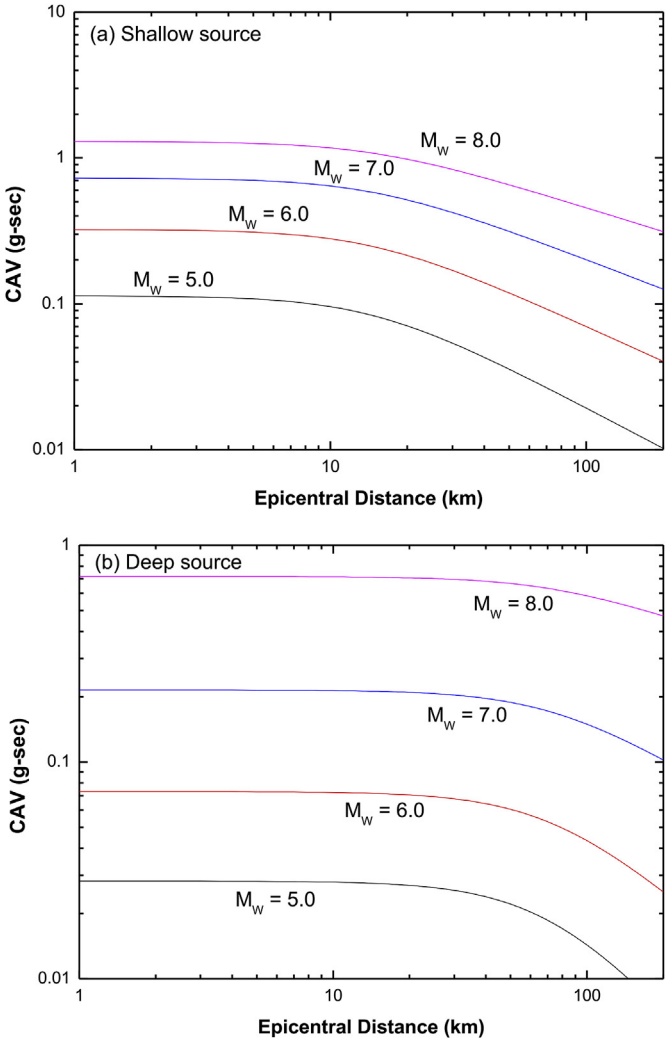

Fig. 13. Median predicted values of CAV with respect to epicentral distance: a) shallow source and b) deep source; note that median predicted CAV value is calculated for Type-D site condition with the Vs30 = 233 m/s.

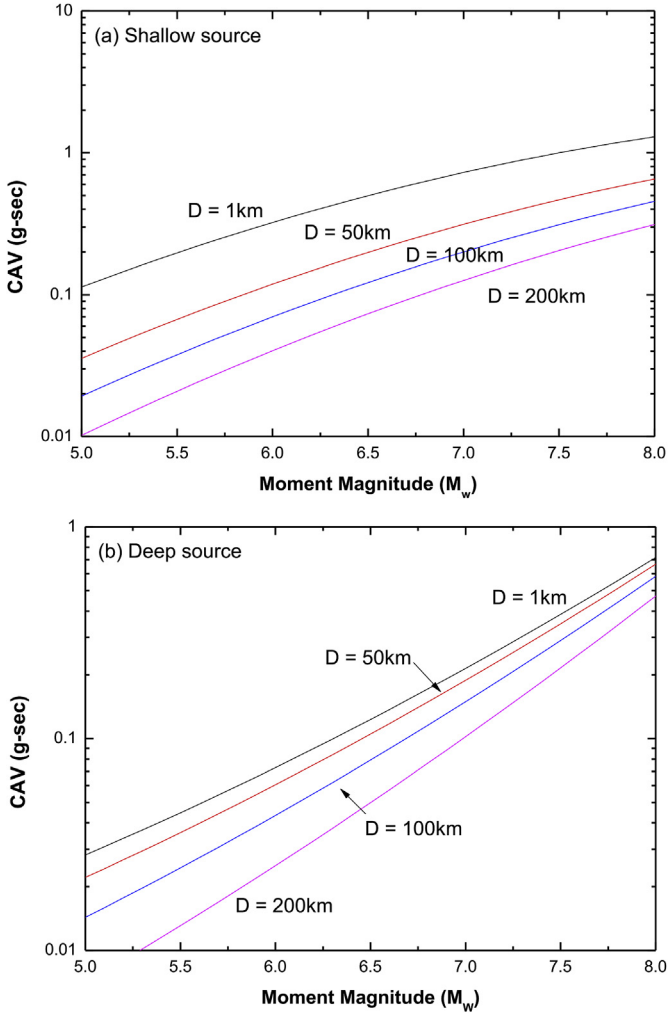

Fig. 14. Median predicted values of CAV with respect to moment magnitude: a) shallow source and b) deep source; note that median predicted CAV value is calculated for Type-D site condition with the Vs30 = 233 m/s.

equal to PGA = f (M_{max}, D_{min}), with some recommending it as PGA = f (M_{max}, D_{min}) + σ_ε with the standard deviation of model error (σ_ε) also taken into account.

Then when a site is surrounded by N_S seismic sources, the maximum of the N_S deterministic seismic hazards is the final estimate of DSHA [1]:

$$PGA = MAX\{PGA_i\} \tag{10}$$

where PGA_i is the deterministic seismic hazard associated with the i-th seismic source.

- Issues with seismic hazard assessment

It is understood that neither PSHA nor DSHA could perfectly predict seismic hazards [e.g., Refs. [51–56]]. It was found that PSHA predictions were quite deviated from our instrumental data/observation [52], while DSHA might underestimate seismic hazard without considering the aleatory uncertainty of a GMPE model [54]. Others include proper/improper use of logic-tree analysis in seismic hazard analysis, and the issue with the assessment's transparency and repeatability, among others [57,58]. The comments summarized here should provide a more complete review on seismic hazard analysis, while it is beyond the scope of this study to justify each of them.

5.2. CAV seismic hazard study for Taipei

As mentioned previously, most seismic hazard studies are PGA- or SA-based using associated GMPEs as the performance function. Therefore, one application of the CAV GMPEs we developed is CAV seismic hazard assessment, estimating the annual rate of CAV exceedance from probabilistic analysis, or the maximum CAV from deterministic analysis. Compared to conventional seismic hazard assessments, the modification is to replace PGA GMPEs with CAV ones.

With the local CAV GMPE and with other seismological/geological data from the literature (i.e., Fig. 18: local seismic source models; Table 2: data summary) [59], we conducted the first CAV seismic hazard analysis for a typical site (121.51°E and 25.03°N; Type-E condition; Vs30 = 160 m/s) in Taipei. Fig. 19 shows the CAV hazard curve for the site, with an annual rate of CAV > 0.97 g-sec about 0.002 per year, or there is a 10% occurrence probability for Taipei to encounter such seismic hazard in 50 years. By contrast, the analysis also suggests an annual rate of 0.078 per year that the city could experience such a seismic hazard. Note that CAV > 0.30 g-sec is considered the threshold of MMI level VII [8].

On the other hand, the DSHA estimate is about 0.60 g-sec in CAV for Taipei, on the basis of the maximum magnitude and minimum distance. More details of the analysis (e.g., maximum earthquake magnitude and shortest epicentral distance of each seismic source) are summarized in Table 3.

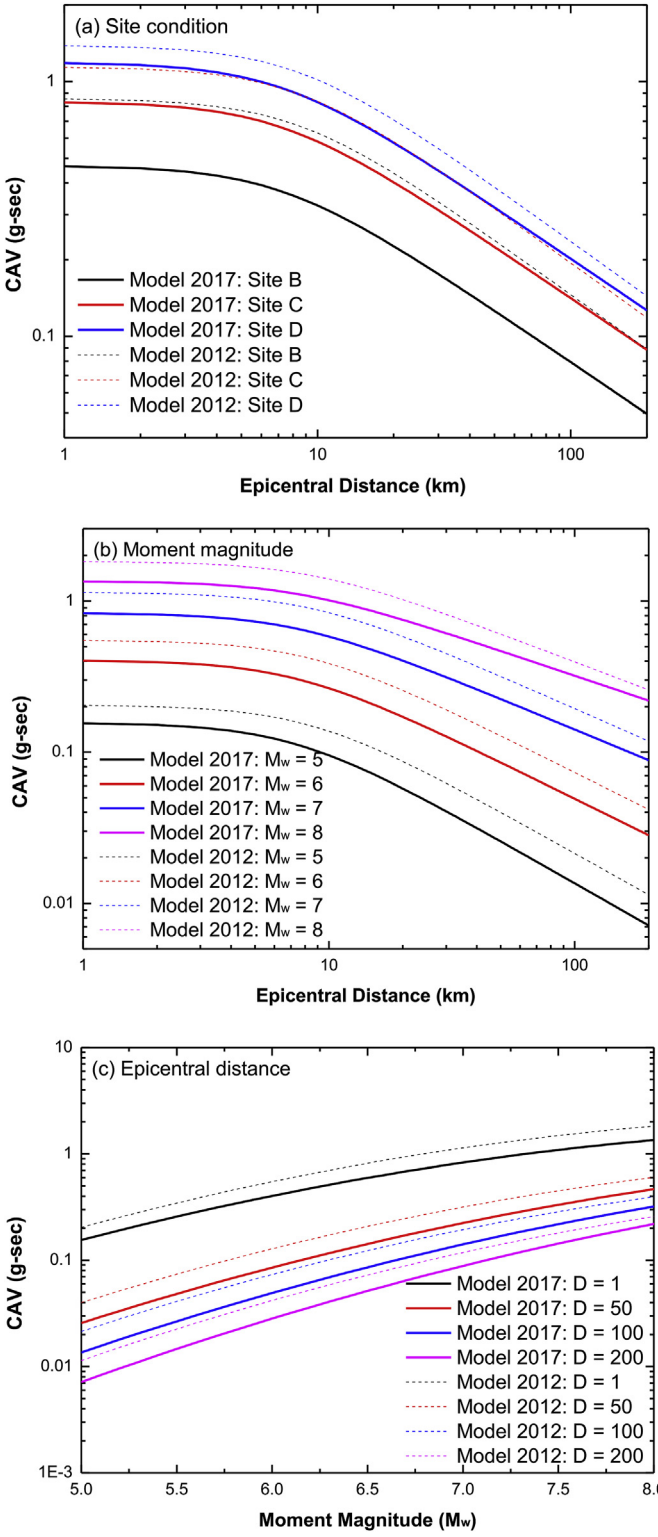

Fig. 15. Comparison between Model 2017 (this study) and Model 2012: a) median values calculated for different site condition given $M_W = 7$, b) median values calculated given different moment magnitude for Type-C site condition, and c) median values calculated given different epicentral distance for Type-C site condition; note that Vs_{30} = 906, 512, 233, 158 m/s is adopted for Type-B, C, D, E site condition, respectively, in Mode 2017, and median values of Model 2012 are calculated referring to normal faulting.

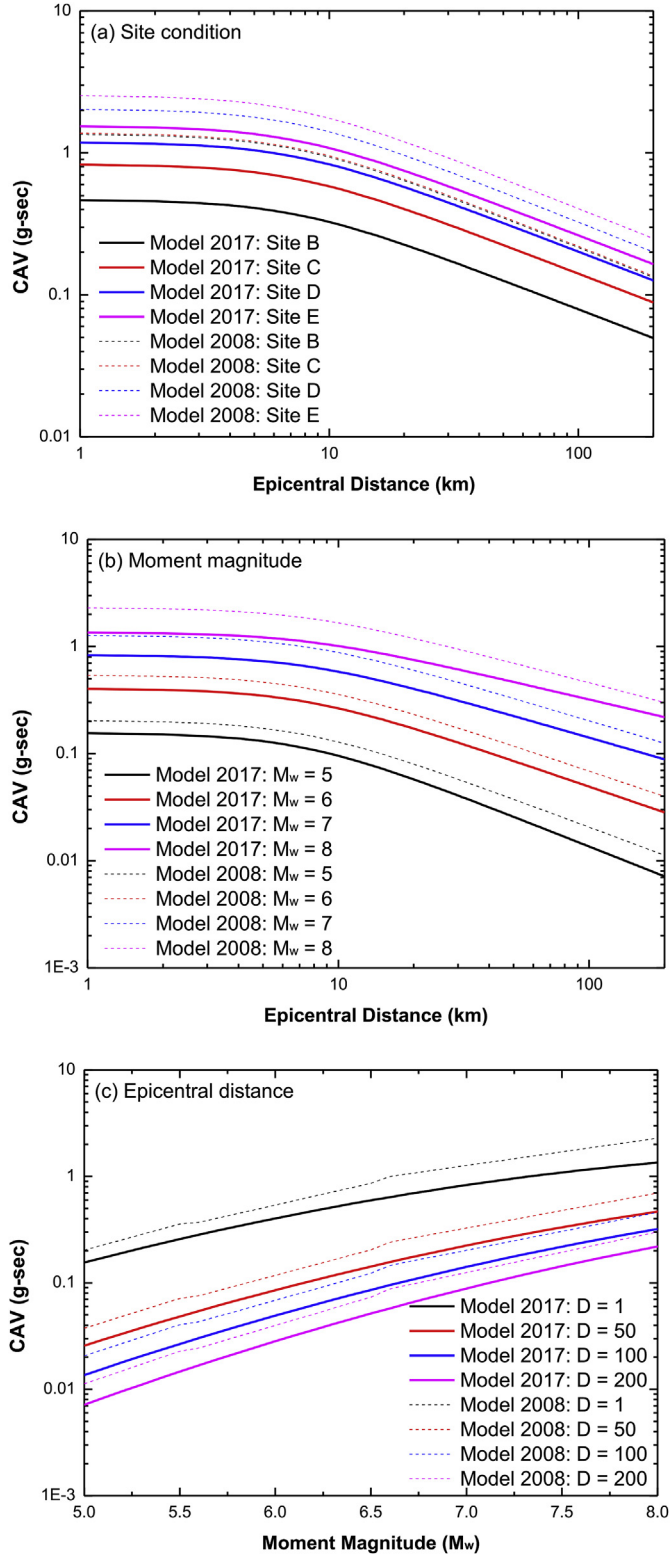

Fig. 16. Comparison between Model 2017 (this study) and Model 2010. Unless otherwise specified, median values are evaluated with $M_W = 7$, normal faulting, Vs_{30} = 906, 512, 233, 158 m/s for Type-B, C, D, E site condition, respectively, $Z_{2.5}$ = 2 km, Z_{TOR} = 10 km, $R_{RUP} = 2R_{JB}$, $|\delta| \leq 70°$

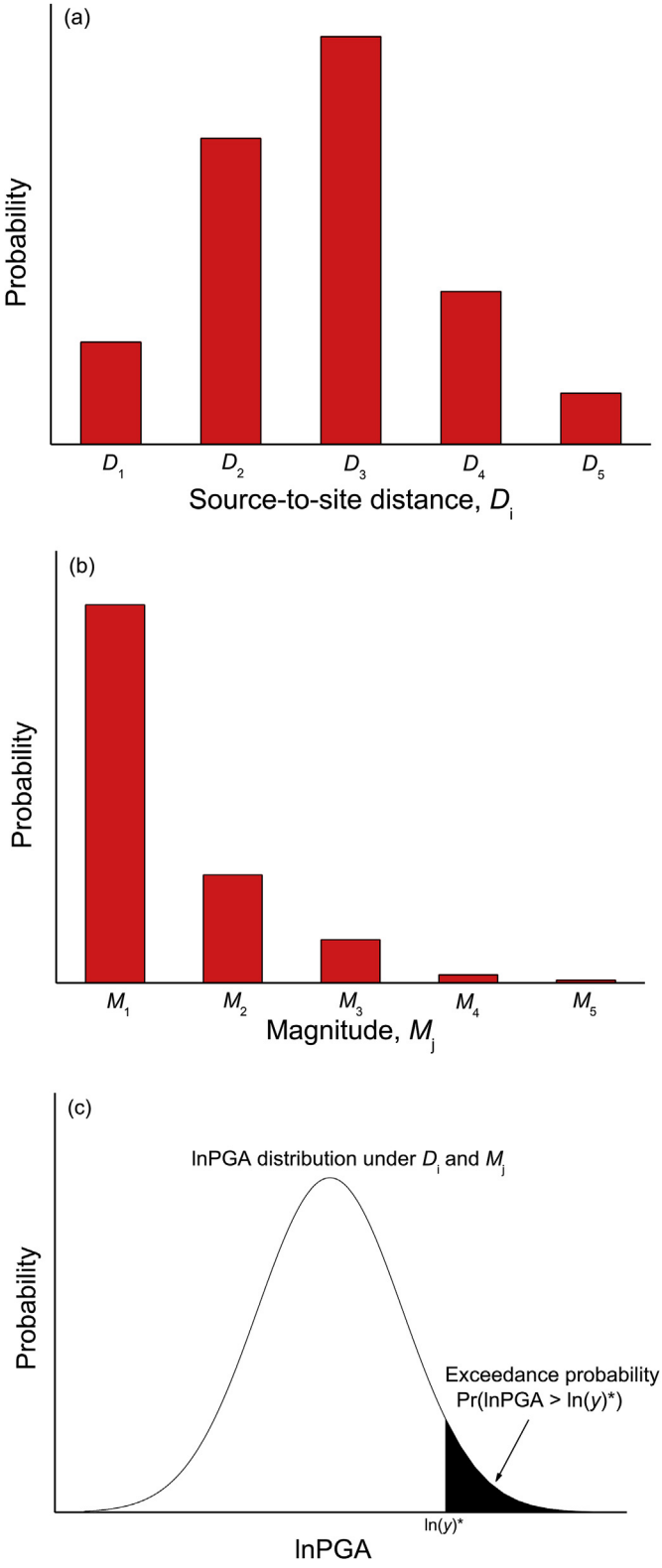

Fig. 17. Systematic diagram illustrating the basics of PSHA algorithms: a) distribution of source-to-site distance, b) distribution of magnitude, and c) lnPGA distribution from GMPE under a given magnitude and distance, and the exceedance probability as the shaded area.

5.3. PGA-CAV joint seismic hazard assessment and future study

To the best of our knowledge, not an earthquake-resistant design uses CAV as the only criterion to design/build structures capable of withstanding ground motions with CAV > 0.16, g-sec, 0.3 g-sec, etc. As a result of that, it requires more future studies to explore how to implement CAV seismic hazard analysis into earthquake-resistant design, as some studies pointed out [60–63].

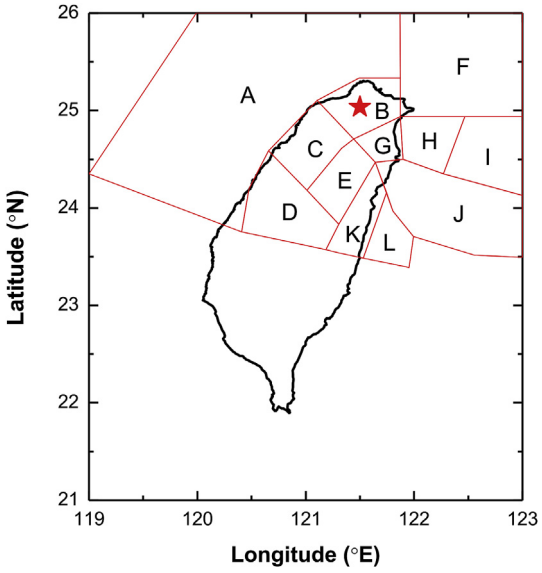

Fig. 18. Locations of the study site (121.51°E, 25.03°N) and the 12 seismic sources within 200 km from the site [59].

Table 2
Summary of the 12 area sources within 200 km from the study site; the *a*-value and *b*-value are the parameters of the Gutenberg-Richter recurrence law ([59]).

Source zone	*a*-value	*b*-value	Maximum magnitude (M_w)
A	3.100	0.849	6.6
B	2.579	0.800	6.4
C	3.137	0.916	5.0
D	3.118	0.740	6.5
E	1.914	0.577	6.5
F	2.163	0.689	6.5
G	2.236	0.638	6.5
H	2.453	0.593	7.6
I	3.270	0.658	7.6
J	3.249	0.644	7.0
K	1.943	0.520	6.5
L	2.962	0.681	7.5

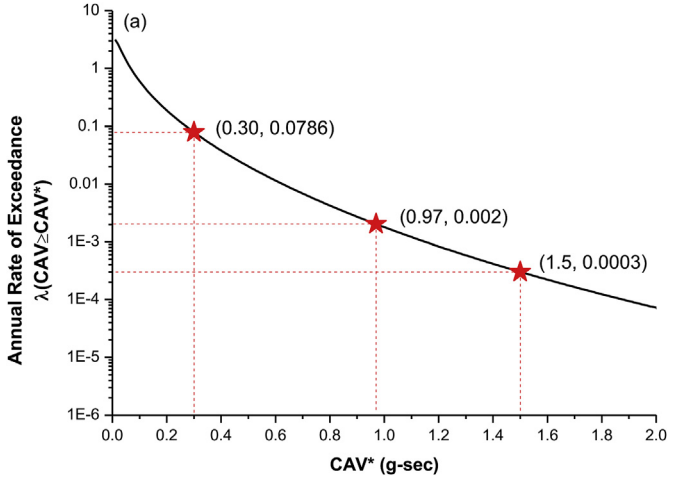

Fig. 19. CAV seismic hazard curve for Taipei (121.51°E and 25.03°N; Type-E site condition; Vs30 = 160 m/s).

Table 3
Summary of the deterministic CAV hazard assessment for the study site at Taipei; note that the site is located within Zone H and the focal depth is assumed at 15 km.

Source zone	Maximum earthquake magnitude (M_W)	Shortest epicentral distance (km)	Deterministic estimate of CAV (g-sec)
A	6.6	28.80	0.322
B	6.4	0.00	0.480
C	5.0	28.50	0.058
D	6.5	98.89	0.128
E	6.5	38.28	0.247
F	6.5	36.89	0.253
G	6.5	28.34	0.297
H	7.6	38.80	**0.600**
I	7.6	95.45	0.362
J	7.0	64.83	0.278
K	6.5	65.49	0.172
L	7.5	102.41	0.320

For example, PGA-CAV joint (probabilistic) seismic hazard assessment that calculates the PGA-CAV exceedance probability, Pr (PGA > pga* and CAV > cav*), is considered an improvement over the conventional PGA- or SA-based approach. Specifically, EPRI proposed CAV 0.16 g-sec as a threshold for such PGA-CAV joint assessments that aim to estimate the annual rate of PGA > pga* and CAV > 0.16 g-sec with the additional criterion (i.e., CAV > 0.16 g-sec). In addition, the correlation between CAV and PGA/SA was also investigated, which should help select/develop site-specific ground motions for some earthquake-resistant design [62].

Theoretically speaking, the PGA-CAV joint seismic hazard study should not be that difficult to be implemented because the methodology is the almost same as the conventional assessment. The key technical issue is how to develop PGA-CAV joint probability distributions subject to a given pair of magnitude and distance. Although some “prototype” methods were proposed for resolving the calculation, more justification with field data is need [e.g., 60, 63].

We also consider the PGA-CAV seismic hazard study should be better than the current model, and the methodology is worth studying in the future. Recently, it was found that PGA-CAV joint probability functions can be well modeled by the copula theory/approach [34], and this could be useful to the developments of PGA-CAV joint probability distributions, then facilitating PGA-CAV seismic hazard assessments.

6. Summary

Based on data from a local strong-motion database in Taiwan, this study developed the first local CAV GMPEs for the study area, including model checking and model comparison. Also note that the empirical model developed was based on 24,667 strong-motion records, the largest sample size by far for such a study.

The paper also presents the first CAV seismic hazard assessment for Taipei, using the local CAV GMPE we developed. The probabilistic analysis shows that the annual rate for the city to encounter a ground motion with CAV > 0.97 g-sec is about 0.002 per year, or there is a 10% occurrence probability for such a seismic hazard to recur in 50 years. By contrast, the deterministic, scenario-based analysis suggests the CAV estimate be 0.60 g-sec for the study area.

Acknowledgements

We appreciate the Editor and the reviewer for the review and constructive comments, making the submission much improved in so many aspects. We are thankful to the Central Weather Bureau Taiwan for providing data for this study. We also appreciate the financial support from the Ministry of Science and Technology, Republic of China (Taiwan) on this research (Grant: MOST106-2218-E-008-013-MY2).

References

[1] Kramer SL. Geotechnical earthquake engineering. N. J.: Prentice Hall Inc.; 1996.
[2] Abrahamson N, Silva W. Summary of the Abrahamson & silva NGA ground-motion relations. Earthq Spectra 2008;24:67–97.
[3] Boore DM, Atkinson GM. Ground-motion prediction equations for the average horizontal component of PGA, PGV, and 5%-damped PSA at spectral periods between 0.01 s and 10.0 s. Earthq Spectra 2008;24:99–138.
[4] Campbell KW, Bozorgnia Y. NGA ground motion model for the geometric mean horizontal component of PGA, PGV, PGD and 5% damped linear elastic response spectra for periods ranging from 0.01 to 10 s. Earthq Spectra 2008;24:139–71.
[5] Chiou BJ, Youngs RR. An NGA model for the average horizontal component of peak ground motion and response spectra. Earthq Spectra 2008;24:173–215.
[6] Danciu L, Tselentis G. Engineering ground-motion parameters attenuation relationships for Greece. Bull Seismol Soc Am 2007;97:162–83.
[7] Lin PS, Lee CT, Cheng CT, Sung CH. Response spectral attenuation relations for shallow crustal earthquakes in Taiwan. Eng Geol 2011;121:150–64.
[8] Electric Power Research Institute (EPRI). A criterion for determining exceedance of the operating basis earthquake. Report NP-5930, Palo Alto, California. 1988.
[9] Electric Power Research Institute (EPRI). Standardization of the cumulative absolute velocity. Report TR-100082, Palo Alto, California. 1991.
[10] Cabañas L, Benito B, Herráiz M. An approach to the measurement of the potential structural damage of earthquake ground motions. Earthq Eng Struct Dyn 1997;26:79–92.
[11] Kramer SL, Mitchell RA. Ground motion intensity measures for liquefaction hazard evaluation. Earthq Spectra 2006;22:413–38.
[12] Koliopoulos PK, Margaris BN, Klimis NS. Duration and energy characteristics of Greek strong motion records. J Earthq Eng 1998;2:390–417.
[13] Housner GW. Behavior of structures during earthquakes. J Eng Mech Div ASCE 1959;85:104–29.
[14] Kostov M. Site specific estimation of cumulative absolute velocity. Proceeding of 18th international conference on structural mechanics in reactor technology. Beijing, China: SMiRT 18; 2005. p. 3041–50.
[15] Campbell KW, Bozorgnia Y. Cumulative absolute velocity (CAV) and seismic intensity based on the PEER-NGA database. Earthq Spectra 2012;28:457–85.
[16] Campbell KW, Bozorgnia Y. A ground motion prediction equation for the horizontal component of cumulative absolute velocity (CAV) based on the PEER-NGA strong motion database. Earthq Spectra 2010;26:635–50.
[17] Campbell KW, Bozorgnia Y. Prediction equations for the standardized version of cumulative absolute velocity as adapted for use in the shutdown of US nuclear power plants. Nucl Eng Des 2011;241:2558–69.
[18] Du W, Wang G. A simple ground-motion prediction model for cumulative absolute velocity and model validation. Earthquake Eng Struc 2013;42:1189–202.
[19] Campbell KW, Bozorgnia Y. A comparison of ground motion prediction equations for Arias intensity and cumulative absolute velocity developed using a consistent database and functional form. Earthq Spectra 2012;28:931–41.
[20] Wang JP, Wu YM. A new seismic hazard analysis using FOSM algorithms. Soil Dynam Earthq Eng 2014;67:251–6.
[21] Hsiao NC, Wu YM, Zhao L, Chen DY, Huang WT, Kuo KH, Shin TC, Leu PL. A new prototype system for earthquake early warning in Taiwan. Soil Dynam Earthq Eng 2011;31:201–8.
[22] Wang JP, Huang D, Yang Z. The deterministic seismic hazard map for Taiwan developed using an in-house Excel-based program. Comput Geosci 2012;48:111–6.
[23] Wang JP, Huang D, Cheng CT, Shao KS, Wu YC, Chang CW. Seismic hazard analysis for Taipei City including deaggregation, design spectra, and time history with Excel applications. Comput Geosci 2013;52:146–54.
[24] Wu YM, Chen CC. Seismic reversal pattern for the 1999 Chi-Chi, Taiwan, Mw 7.6 earthquake. Tectonophysics 2007;429:125–32.
[25] Wu YM, Chen CC, Zhao L, Chang CH. Seismicity characteristics before the 2003 Chengkung, Taiwan earthquake. Tectonophysics 2008;457:177–82.
[26] Chen CH, Wang JP, Wu YM, Chan CH, Chang CH. A study of earthquake interoccurrence times distribution models in Taiwan. Nat Hazards 2013;69:1335–50.
[27] Central CWB. Weather Bureau Taiwan. Available from: http://www.cwb.gov.tw/V7/earthquake/accsta.htm, Accessed date: April 2016.
[28] Shin TC, Tsai YB, Yeh YT, Liu CC, Wu YM. Strong-motion instrumentation programs in Taiwan. International Handbook of Earthquake and Engineering Seismology 2003;81B:1057–62.
[29] Wen KL, Shin TC, Wu YM, Hsiao NC, Wu BR. Earthquake early warning technology progress in Taiwan. J Disaster Res 2009;4:202–10.
[30] Kuo CH, Wen KL, Hsieh HH, Lin CM, Chang TM, Kuo KW. Site classification and Vs30 estimation of free-field TSMIP stations using the logging data of EGDT. Eng Geol 2012;129–130:68–75.
[31] Sokolov VY, Loh CH, Wen KL. Empirical models for site and region-dependent ground-motion parameters in the Taipei area: a unified approach. Earthq Spectra 2001;17:313–31.
[32] Wu YM, Teng TL, Hsiao NC, Chin TC, Lee WHK, Tsai YB. Progress on earthquake rapid reporting and early warning systems in Taiwan. Earthquake hazard, risk, and strong ground motion. Beijing: Seismological Press; 2004. p. 463–86.
[33] Xu Y, Wang JP, Wu YM, Kuo-Chen H. Reliability assessment on earthquake early warning: a case study from Taiwan. Soil Dynam Earthq Eng 2017;92:397–407.
[34] Xu Y, Tang XS, Wang JP, Kuo-Chen H. Copula-based joint probability function for PGA and CAV: a case study from Taiwan. Earthq Eng Struct Dyn 2016;13:2123–36.
[35] Wu YM, Shin TC, Chang CH. Near real-time mapping of peak ground acceleration

and peak ground velocity following a strong earthquake. Bull Seismol Soc Am 2001;91:1218–28.
[36] Abrahamson A, Youngs RR. A stable algorithm for regression analyses using the random effects model. Bull Seismol Soc Am 1992;82:505–10.
[37] Devore JL. Probability and statistics for engineering and the science. Brooks/Cole, Cengage Learning; 2012.
[38] Wang JP, Xu Y, Wu YM. A FOSM calculation for seismic hazard assessment with the consideration of uncertain size conversion. Nat Hazard Earth Sys 2013;13:2649–57.
[39] Mualchin L. Seismic hazard analysis for critical infrastructures in California. Eng Geol 2005;79:177–84.
[40] Cheng CT, Chiou SJ, Lee CT, Tsai YB. Study on probabilistic seismic hazard maps of Taiwan after Chi-Chi earthquake. J GeoEng 2007;2:19–28.
[41] Aldama-Bustos G, Bommer JJ, Fenton CH, Stanford PJ. Probabilistic seismic hazard analysis for rock sites in the cities of Abu Dhabi, Dubai and Ra's Al Khaymah, United Arab Emirates. Georisk 2009;3:1–29.
[42] Roshan AD, Basu PC. Application of PSHA in low seismic region: a case study on NPP site in peninsular India. Nucl Eng Des 2010;240:3443–54.
[43] Sitharam TG, Kolathayar S. Seismic hazard analysis of India using areal sources. J Asian Earth Sci 2013;62:647–53.
[44] Wang JP, Taheri H. A seismic hazard analysis for the region of Tehran. Nat Hazards Rev ASCE 2014;15:121–7.
[45] United States Nuclear Regulatory Commission (USNRC). Identification and characterization of seismic sources and determination of safe shutdown earthquake ground motion. Regulatory Guide 1997;1. 165.
[46] Graves R, Jordan TH, Callaghan S, Deelman E, Field E, Juve G, Kesselman C, Maechling P, Mehta G, Milner K, Okaya D, Small P, Vahi K. CyberShake: a physics-based seismic hazard model for southern California. Pure Appl Geophys 2011;168:367–81.
[47] Thenhaus PC, Campbell KW. Seismic hazard analysis. In: Chen WF, Scawthorn C, editors. Earthquake engineering handbook. Boca Raton, FL: CRC Press; 2004 [Chapter 8].
[48] McGuire RK. Seismic hazard and risk analysis. EERI monograph No, MNO-10 earthquake engineering research Institute, EL cerrito, CA. 2004.
[49] Musson RMW. Intensity-based seismic risk assessment. Soil Dynam Earthq Eng 2000;20:353–60.
[50] Wang JP, Wu MH. Risk assessments on active faults in Taiwan. Bull Eng Geol Environ 2015;74:117–24.
[51] McGuire RK. Deterministic vs. probabilistic earthquake hazards and risks. Soil Dynam Earthq Eng 2001;21:377–84.
[52] Castaños H, Lomnitz C. PSHA: is it science? Eng Geol 2002;66:315–7.
[53] Bommer JJ. Deterministic vs. probabilistic seismic hazard assessment: an exaggerated and obstructive dichotomy. J Earthq Eng 2002;6:43–73.
[54] Bommer J. Uncertainty about the uncertainty in seismic hazard analysis. Eng Geol 2003;70:165–8.
[55] Krintzsky E. How to combine deterministic and probabilistic methods for assessing earthquake hazards. Eng Geol 2003;70:157–63.
[56] Klügel JU. Error inflation in probabilistic seismic hazard analysis. Eng Geol 2007;90:186–92.
[57] Klügel JU. Seismic hazard analysis-Quo vadis? Earth Sci Rev 2008;88:1–32.
[58] Krinitzsky EL. Problems with logic trees in earthquake hazard evaluation. Eng Geol 1995;39:1–3.
[59] Cheng CT. Uncertainty analysis and de-aggregation of seismic hazard in Taiwan. Chung-Li, Taiwan: Ph.D. Dissertation, Institute of Geophysics, National Central University; 2002. (in Chinese).
[60] Electric Power Research Institute (EPRI). Program on technology innovation: use of cumulative absolute velocity (CAV) in determining effects of small magnitude earthquakes on seismic hazard analyses. Report No. 1014099, Palo Alto, California. 2006.
[61] Watson-Lamprey JA, Abrahamson NA. Use of minimum CAV in seismic hazard analyses. Proc 9th Canadian conference on earthquake engineering, ottawa. 2007. p. 352–8.
[62] Bradley BA. Empirical correlations between cumulative absolute velocity and amplitude-based ground motion intensity measures. Earthq Spectra 2012;28:37–54.
[63] Campbell KW, Bozorgnia Y. Prediction equations for the standardized version of cumulative absolute velocity as adapted for use in the shutdown of US nuclear power plants. Nucl Eng Des 2011;241:2558–69.